NJC

PAPER

Cite this: *New J. Chem.*, 2018, **42**, 1347

New coordination polymers based on 2-methylimidazole and transition metal nitroprusside containing building blocks: synthesis, structure and magnetic properties†

A. Di Santo,[a] H. Osiry,[b] E. Reguera,[b] P. Alborés,‡[c] R. E. Carbonio,‡[d] A. Ben Altabef‡[a] and Diego M. Gil‡*[a]

Received 19th September 2017,
Accepted 15th December 2017

DOI: 10.1039/c7nj03585c

rsc.li/njc

Four coordination polymers obtained by the intercalation of 2-methylimidazole into transition metal nitroprussides T[Fe(CN)$_5$NO] with T = Mn, Fe, Co and Ni were synthesized and characterized. The resulting hybrid inorganic–organic solids crystallize as dihydrates. All the solids were crystallized in an orthorhombic crystal system in the space group $P2_12_12_1$. Their crystal structures were solved and refined from X-ray diffraction data, complemented by structural information derived from spectroscopic (IR, Raman and UV-Vis) and thermal data. The intercalated molecules occupy the axial coordination sites of the metal T(II), while the Fe atom of the nitroprusside anion preserves the octahedral coordination geometry. In the interlayer region, the intercalated molecules retain their interaction through π-stacking interactions. The magnetic measurements indicate that all the solids show antiferromagnetic interactions at low temperatures due to intra-sheet antiferromagnetic exchange interactions of moderate strength. Only complexes with Fe(II) and Mn(II) show long-range inter-sheet ferromagnetic ordering.

1. Introduction

Coordination polymers (CPs) are infinite systems built from metal ion and organic ligand building blocks, which are linked by coordination bonds and other weak chemical interactions. In many cases, a correlation between the detailed synthesis conditions and structural features is very difficult to draw, and the metal ions selected play an important role in the determination of the chemical properties of CPs. The development of CPs in materials science, crystal engineering and supramolecular chemistry are areas of research, and the study of their crystal structures has been attracting considerable attention in the last decade due to their potential application in the fields of catalysis,[1] luminescence materials,[2] sensors[3,4] and gas storage.[5] Some magnetic CPs have been reported in the literature and they show a wide variety of magnetic properties such as ferromagnetism at room and low temperature,[6–8] and spin crossover.[9–11]

The intercalation of organic molecules in a layered solid is a useful method to study the non-covalent interactions (π···π, C–H···π or hydrogen bonding) between neighboring molecules. Self-assembly of molecular building blocks through molecular recognition has led the way in the design and preparation of various functional materials of both organic and hybrid organic–inorganic types. In the solid formed, there are two ways of electronic communication or interaction between the metal centers, one of them is within the layer and the other between the neighboring layers through intercalated molecules. These magnetic interactions could be of antiferromagnetic or ferromagnetic nature, depending on the ligands involved. When π-stacking interactions between neighboring molecules are present, the interaction is of a ferromagnetic nature, as was found in different layered materials.[8]

Recently, we became interested in the intercalation of nitrogen-containing ligands in transition metal tetracyanonickelates(II) and nitroprussides.[8,12–15] The intercalation of imidazole derivatives and thiazole in T[Ni(CN)$_4$] layers (T = Mn, Fe, Co, and Ni) produced hybrid inorganic–organic materials with

[a] *INQUINOA (CONICET-UNT). Instituto de Química Física, Facultad de Bioquímica, Química y Farmacia. Universidad Nacional de Tucumán, San Lorenzo 456, T4000CAN San Miguel de Tucumán, Argentina. E-mail: dmgil@fbqf.unt.edu.ar*
[b] *Centro de Investigación en Ciencia Aplicada y Tecnología Avanzada, Unidad Legaria, Instituto Politécnico Nacional, Mexico*
[c] *Departamento de Química Inorgánica, Analítica y Química Física, INQUIMAE, Facultad de Ciencias Exactas y Naturales, Universidad de Buenos Aires, Pabellón 2, Ciudad Universitaria, C1428EHA Buenos Aires, Argentina*
[d] *INFIQC (CONICET-UNC), Departamento de Fisicoquímica, Facultad de Ciencias Químicas, Universidad Nacional de Córdoba, Haya de la Torre esquina Medina Allende, Ciudad Universitaria, X5000HUA Córdoba, Argentina*

† Electronic supplementary information (ESI) available. CCDC 1437640–1437642 and 1572511. For ESI and crystallographic data in CIF or other electronic format see DOI: 10.1039/c7nj03585c

‡ Members of the Research Career of CONICET.

3D structures. In these compounds, the layers were stabilized by π-stacking interactions, and the magnetic behavior observed in this series of compounds was determined by the co-existence of two types of interactions between the metal centers.[8,12,13]

Compounds containing the nitroprusside anion provide a rich variety of photo-physical properties. Combined with a suitable paramagnetic transition metal ion, the nitroprusside complexes become more interesting due to the magneto-optical correlation. In addition, the incorporation of the nitroprusside anion can result in various molecular dimensionalities of the metal complexes, which is of great interest in supramolecular chemistry. On the other hand, the incorporation of imidazole during the preparation of transition metal nitroprussides inhibits the coordination of the axial CN groups to the metal center, and layered 2D structures can form. The existence of π-stacking interactions of the aromatic rings from neighboring molecules produces magnetic interactions between T(II) cations located in neighboring layers.[14,15]

Herein, we report the synthesis, and structural and magnetic characterization of a series of layered 2D transition metal nitroprussides obtained by the intercalation of 2-methylimidazole (2-MeIm). The crystal structures of the synthesized compounds were solved and refined using powder X-ray diffraction (PXRD) measurements complemented by thermogravimetric and differential thermal analysis measurements and spectroscopic data (IR, Raman and UV-Vis). The interaction between the 2-MeIm ligands was evaluated from the refined crystal structures and low temperature magnetic measurements.

2. Experimental

2.1. Synthesis

The samples under study were obtained by a co-precipitation method, by mixing aqueous solutions of sodium nitroprusside (1 mmol), 2-MeIm (2 mmol) and TCl_2 ($T = Mn^{2+}$, Ni^{2+}, and Co^{2+}) and $Fe(NH_4)_2(SO_4)_2$ for $T = Fe^{2+}$. In the case of the Fe(II) complex, ascorbic acid was added in order to prevent the oxidation of the metal. The fine solids thus formed were aged for a week and then the precipitates were separated by filtration and washed several times with distilled water to remove the non-reacted salts. For all of the compounds, only very small and twinned crystals of low X-ray scattering ability were obtained and, thus, their crystal structures were determined by Rietveld refinement (see Section 2.3). The nature of the solids formed was established from elemental analysis, PXRD, IR, Raman, UV-Vis and thermal data.

$Mn(2\text{-MeIm})_2[Fe(CN)_5NO]\cdot 2H_2O$ ($Mn(2\text{-MeIm})_2NP$). Orange powder. Yield: 80%. Anal. calc. for $MnFeC_{13}H_{16}N_{10}O_3$: C, 33.1; H, 3.39; N, 29.7. Found: C, 33.0; H, 3.42; N, 29.6%.

$Fe(2\text{-MeIm})_2[Fe(CN)_5NO]\cdot 2H_2O$ ($Fe(2\text{-MeIm})_2NP$). Green powder. Yield: 85%. Anal. calc. for $Fe_2C_{13}H_{16}N_{10}O_3$: C, 33.1; H, 3.39; N, 29.7. Found: C, 33.2; H, 3.40; N, 29.6%.

$Ni(2\text{-MeIm})_2[Fe(CN)_5NO]\cdot 2H_2O$ ($Ni(2\text{-MeIm})_2NP$). Grey powder. Yield: 90%. Anal. calc. for $NiFeC_{13}H_{16}N_{10}O_3$: C, 32.9; H, 3.37; N, 29.5. Found: C, 32.8; H, 3.39; N, 29.4%.

$Co(2\text{-MeIm})_2[Fe(CN)_5NO]\cdot 2H_2O$ ($Co(2\text{-MeIm})_2NP$). Pink powder. Yield: 70%. Anal. calc. for $CoFeC_{13}H_{16}N_{10}O_3$: C, 32.9; H, 3.37; N, 29.5. Found: C, 32.7; H, 3.36; N, 29.4%.

2.2. Instrumentation

Elemental analysis for carbon, hydrogen and nitrogen was performed using a Carlo Erba EA1108 analyzer. The IR absorption spectra of the solids were recorded in KBr pellets, using an FTIR PerkinElmer GX1 in the 4000–400 cm^{-1} frequency range. Raman spectra were recorded at the 3500–50 cm^{-1} interval using a ThermoScientific DXR Raman microscope. Raman data were collected using a diode-pump, solid-state laser of 532 nm at a resolution of 5 cm^{-1}. UV-Vis spectra were recorded on Perkin-Elmer equipment using the integration sphere method. Thermogravimetric (TGA) and differential thermal analysis (DTA) measurements were performed using a Shimadzu DTG-60 thermo-balance in the temperature range of 25–800 °C at a heating rate of 5° min^{-1} under an air flow. The low-temperature zero-field cooling (ZFC) and field cooling (FC) curves were collected using a MPM-3 magnetometer from Quantum Design, under an applied field of 80 Oe, in the temperature range of 1.8–300 K. The effective magnetic moment (μ_{eff}) was calculated according to $\mu_{eff} = 2.828\,\mathrm{sqrt}(\chi_M T)$, considering the diamagnetic corrections for the involved atoms.

2.3. Powder X-ray data collection and refinement

PXRD patterns were recorded with Cu-Kα1 radiation with $\lambda = 1.5406$ Å in the Bragg–Brentano geometry by using a D8 Advance diffractometer (Bruker) equipped with a Lynx eye detector and a germanium monochromator for high-resolution measurements. In order to index the PXRD patterns and to identify the unit cell parameters, the DICVOL method[16] was used. DICVOL is an indexing program included within the complete FullProf package based on the exhaustive volumetric dichotomy approach. The indexing strategy is based on the search for a solution with a variation of parameters from high to low symmetry using partitioning of the unit cell volume in 400 A^3 increments. A possible solution is found when a unit cell produces the calculated diffraction peaks close to the observed diffraction peaks.[16] For the structural study, the diffraction patterns were decomposed, in terms of extracted intensities, by the Le Bail procedure using the pseudo-Voigt peak profile function.[17] The structural model was obtained by the combination of direct and heavy atom methods implemented in the SHELX program.[18] The structural model was completed by the analysis of the electron density Fourier maps. The final structural model thus obtained was refined by using the Rietveld method[19] with the FullProf program,[20] taking into account the interatomic distances C–N, Fe–C, N–O and Fe–N reported in the literature for different transition metal nitroprussides.[21,22] The details of the data collection, crystal data and structure refinement for T(2-MeIm)2[Fe(CN)$_5$NO]·nH_2O (T = Mn, Fe, Co, and Ni) are shown in Table 1. In the case of layered solids of transition metal nitroprussides under study, the building block $[Fe(CN)_5NO]^{2-}$ and the 2-methylimidazole molecule to be intercalated were treated as rigid bodies. The FullProf program incorporates the rigid body

Table 1 Details of data collection, crystal data and structure refinement for T(2-MeIm)$_2$[Fe(CN)$_5$NO]·2H$_2$O (T = Mn, Fe, Co and Ni)

	Mn	Fe	Co	Ni
Diffractometer	D8 Advance	D8 Advance	D8 Advance	D8 Advance
Radiation	CuK$_{\alpha1}$	CuK$_{\alpha1}$	CuK$_{\alpha1}$	CuK$_{\alpha1}$
2θ range [°]	5–80	5–80	5–80	5–65
Step scan [°]	0.008	0.008	0.008	0.018
Count time [s per step]	10	10	10	10
Crystal system	Orthorhombic	Orthorhombic	Orthorhombic	Orthorhombic
Space group	$P2_12_12_1$	$P2_12_12_1$	$P2_12_12_1$	$P2_12_12_1$
a [Å]	19.1652(2)	19.0271(4)	19.0000(5)	19.0005(2)
b [Å]	15.1252(4)	14.9773(5)	14.9003(5)	14.7563(1)
c [Å]	7.3394(1)	7.2490(1)	7.1784(2)	7.1233(5)
α [°]	90	90	90	90
β [°]	90	90	90	90
γ [°]	90	90	90	90
V [Å^3]	2127.53(7)	2065.78(9)	2032.25(10)	1997.23(14)
Z	4	4	4	4
Number of observations	1287	1248	1222	476
Number of reflections	438	438	319	266
Number of structural parameters refined[a]	39	39	39	39
Number of profile parameters refined	12	12	12	12
Number of distance restrictions	8	8	8	8
R_{exp}	2.404	1.766	2.058	1.23
R_{wp}	3.752	1.794	2.787	2.19
R_B	16.481	14.469	18.946	7.25
S	1.562	1.345	1.352	1.783

[a] Intensities of reflections were calculated using a rigid body.

option of molecular fragments into the structure refinement process using the Rietveld method.[20] The process to introduce rigid body refinement begins once an approximate structure model was obtained which is derived from the combination of direct and heavy atom methods. The 2-methylimidazole molecular fragment considered to be the rigid body was obtained by searching for analogue compounds derived from the single crystal structures in the Cambridge Structural Database (CSD), while the building block [Fe(CN)$_5$NO]$^{2-}$ was obtained from the crystal structure of transition metal nitroprussides already reported. The respective rigid body is oriented and positioned within the crystal structure in which a local cartesian coordinate system as a reference is generated. From this orthonormal and internal system, the displacements and rotations of the molecule as a whole will be made using only six refinable parameters: 3 coordinates of the rigid body center describing the displacement from the origin of the internal cartesian system (Xo, Yo, and Zo), and the 3 Euler angles describing its orientation (Θ, Φ, and χ).[20] Thus, the number of refinable parameters for both the unit block [Fe(CN)$_5$NO]$^{2-}$ and 2-methylimidazole was drastically reduced to 6. In order to determine the linearity degree of the C≡N–T bond, the N atoms were not considered within the rigid body formalism of the [Fe(CN)$_5$NO]$^{2-}$ building blocks, since this chain is more flexible. In early stages, the interatomic C≡N distance restraints of 1.145(11) Å were obtained from the *a priori* crystal structure of the transition metal nitroprussides. This restriction was then progressively removed until a more stable refinement was obtained, as premature removal often impedes further progress. Data on the crystal structures solved from powder XRD measurements have been deposited at the Cambridge Crystallographic Data Centre (CCDC): CCDC 1572511 for (Ni), 1437640 (Mn), 1437641 (Fe) and 1437642 (Co).†

3. Results and discussion

3.1. Crystal structures

Fig. 1 shows the experimental and fitted PXRD patterns and their difference according to the refined structural model for Ni(2-MeIm)$_2$[Fe(CN)$_5$NO]·2H$_2$O. The XRD patterns refined by the Rietveld method for T = Co, Fe, and Mn are shown in the ESI.† The four compounds obtained by the intercalation with 2-methylimidazole crystallize in the orthorhombic crystal system in the $P2_12_12_1$ space group with Z = 4 formula units in the unit cell. The refined crystal structures are in agreement with the spectroscopic data discussed below. All complexes

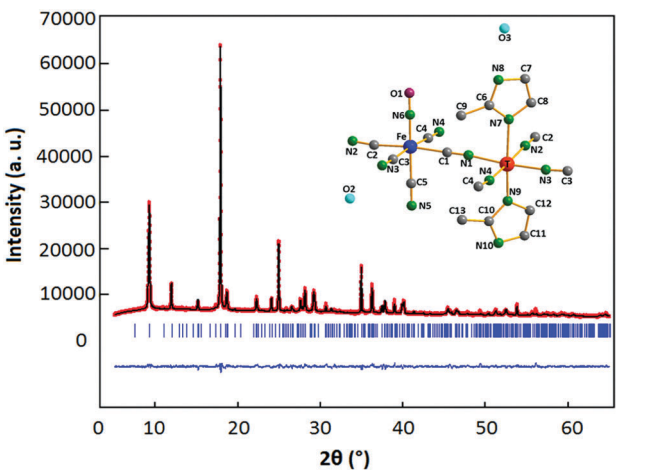

Fig. 1 Experimental and fitted PXRD patterns and their difference according to the refined structural model for Ni(2-MeIm)$_2$[Fe(CN)$_5$NO]·2H$_2$O. Inset: Coordination environment of the involved metal centers (Ni: red and Fe: blue).

Table 2 Relevant geometrical parameters (bond distances and angles) for the series of compounds T(2-MeIm)$_2$[Fe(CN)$_5$NO]·2H$_2$O (T = Mn, Fe, Co and Ni)

T	Polarizing power (Ze/r^2)	Cell volume (Å^3)	T–N$_{MeIm}$ (Å)	Ring–ring distance (Å)	Ring–ring angle (°)
Mn	3.287	2127.53(7)	Mn–N(7): 2.293(8) Mn–N(9): 2.247(8)	4.553	166.47
Fe	3.463	2065.78(9)	Fe(2)–N(7): 2.261(10) Fe(2)–N(9): 2.221(10)	4.502	178.56
Co	3.652	2032.25(10)	Co–N(7): 2.244(4) Co–N(9): 2.226(4)	4.481	175.31
Ni	3.858	1997.23(14)	Ni–N(7): 2.402(16) Ni–N(9): 2.031(16)	4.439	174.55

crystallize as dihydrates. In the crystal structures of all of the compounds, the metal center T(II) is coordinated by four nitrogen atoms of the CN ligands occupying the basic plane of the octahedron and two nitrogen atoms occupying the two apical positions from two 2-methylimidazole ligands with N7–T–N9 bond angles of between 175.3 and 177.2°, forming a distorted octahedral environment. The T–N$_{CN}$ distances vary from 2.008(7) to 2.444(7) Å, and the T–N(Im) bond lengths are between 2.031(16) and 2.402(16) Å, which are close to those in reported literature studies.[14,15]

The relevant geometrical parameters such as interatomic bond distances and angles are listed in Table 2. In accordance with the results reported in Table 2, the cell volume and the T–N(Im) bond distance follows a positive correlation with the metal polarizing ability. For the most polarizing metal (Ni), the smallest cell volume and the shortest T–N(Im) distance were observed.[13–15] The effective polarizing power (Ze/r^2) is a measure of the ability of the metal to receive electron density. According to the values of the T–N(Im) distances, the strongest coordination bond is formed for the Ni compound. As expected, the $[Fe(CN)_5NO]^{2-}$ anion consists of five cyano groups and one nitrosyl (NO) ligand coordinated to a Fe(II) center. Four of the CN groups are located in the equatorial plane, while one CN ligand is axially colinear with the NO group (see Fig. 1, inset). The T(II) and Fe metal centers are linked by CN groups (see Fig. 1, inset).

Fig. 2 shows the atomic packing within the unit cell for the T(2-MeIm)$_2$[Fe(CN)$_5$NO]·2H$_2$O complexes. In the interlayer region, the ring–ring angle for neighboring 2-methylimidazole molecules is below 180°, indicating that the molecules deviate from the coplanar configuration. In previous studies, the intercalation of imidazole and thiazole compounds into $[Ni(CN)_4]^{2-}$ layers produced a sandwich-type configuration.[8,12,13] In the series studied in this work, the steric effects caused by the presence of the unbridged CN and NO ligands in the axial position of the Fe center produced a deviation from the coplanar arrangement in these compounds. The layers are stabilized by a face-to-face configuration favored by the charge concentration on the N atom. The supramolecular assembly also includes the existence of π–π intermolecular interactions involving the 2-methylimidazole ligands between different layers, with centroid-to-centroid distances in the range of 4.439–4.453 Å. As a result, the closest T···T distances in the same chain and between neighboring chains are at around 10 Å in all these compounds. The high value

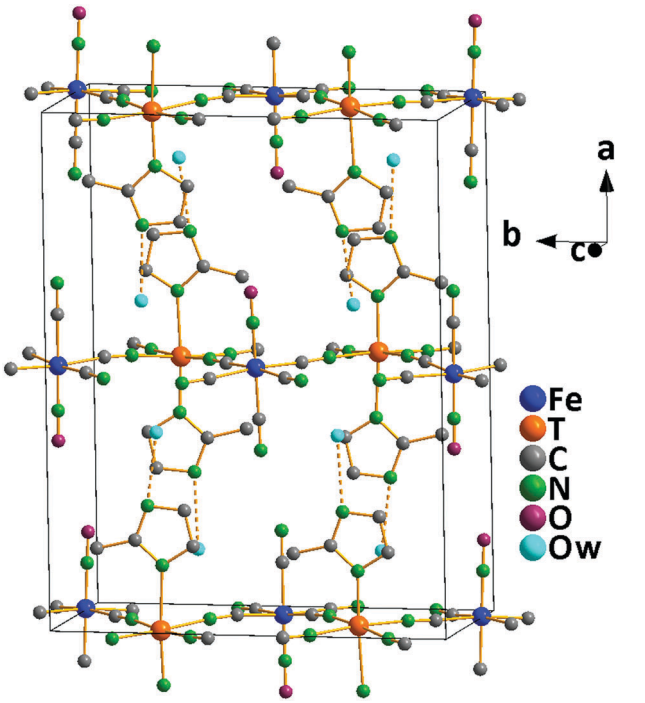

Fig. 2 Atomic packing within the unit cell for the intercalation of 2-methylimidazole to transition metal nitroprussides (T = Mn, Fe, Co and Ni).

of the ring–ring distances for the intercalation of 2-methylimidazole to transition metal nitroprussides suggests that all of the intermolecular interactions could be of a dipolar nature.[14] The orientation of the methyl group for the intercalated molecules is determined by dipolar interactions and steric effects. In the case of the intercalation of 2-ethylimidazole into copper(II) nitroprusside, the orientation of the ethyl group favors the penta-coordination of Cu(II) defined by three CN ligands and the two 2-ethylimidazole molecules.[14] The intermolecular O2–H···N10 (D···A = 2.80(2) Å) and O3–H···N8 (D···A = 2.71(2) Å) interactions are also present in the crystal structure of the solids with T = Mn, Fe, Co and Ni.

3.2. IR, Raman and UV-Vis spectroscopy

The IR and Raman spectra (Fig. 3 and 4, respectively) for all of the compounds in the solid state are consistent with their crystal structures. The assignments of the bands observed in the IR and Raman spectra are shown in the ESI.† The IR spectra

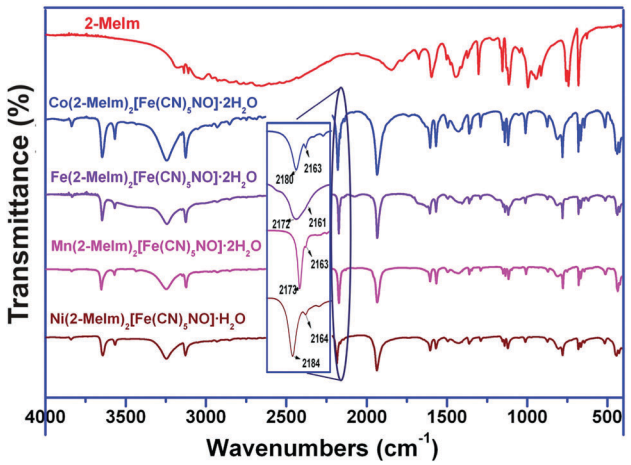

Fig. 3 IR spectra of 2-methylimidazole and the solids T(2-MeIm)$_2$-[Fe(CN)$_5$NO]·2H$_2$O (T = Co, Fe, Mn and Ni). Inset: IR spectra of the CN stretching region.

of the solids present absorptions between 3500 and 3300 cm^{-1} that could be assigned to the O–H stretching modes of water molecules. The absence of broad absorptions for the O–H stretch indicates that the crystallization water molecules do not undergo extensive hydrogen bonding interactions. The band at around 1605 cm^{-1} is assigned to the δ(HOH) bending mode of water molecules. In the IR spectra of 2-MeIm, the strong bands located at 3137 and 3110 cm^{-1} are assigned to the C–H stretching modes of the imidazole ring. These modes appear in the complexes at 3150 and 3125 cm^{-1} for Co(2-MeIm)$_2$NP, 3153 and 3127 cm^{-1} for Ni(2-MeIm)$_2$NP, 3147 and 3123 cm^{-1} for Mn(2-MeIm)$_2$NP and 3150 and 3125 cm^{-1} for Fe(2-MeIm)$_2$NP. The absorption bands of the CH_3 anti-symmetric and symmetric stretching modes are observed in the frequency range of 2966–2930 cm^{-1}. Based on the IR and Raman data, it is possible to propose that the coordination of 2-MeIm to the metal center T(II) occurs through the nitrogen atom of the heterocyclic ring, as already seen in the crystal structures solved from PXRD data discussed previously. When the nitrogen atom of the ring is involved in the complex formation, the ring modes, particularly the modes in the region 1600–1400 cm^{-1}, increase in value due to coupling with T–N bond vibrations. The bands located at 1597, 1303, 1155 and 945 cm^{-1} in the IR spectra of 2-MeIm (1303, 1163 and 939 cm^{-1} in the Raman spectra) are assigned to C–N stretching modes coupled with C–C stretching modes and C–H and N–H bending modes. The remarkable shift at lower frequencies observed for the C–N stretching modes is a diagnostic for the weakening of the C–N bond, which can be caused by the coordination of the nitrogen atom of the imidazole ring to the metal center T(II). The polarizing power measures the ability of the metal to subtract the electronic charge from the ligand and, therefore, to enhance the metal–ligand coordination bond. This explains the higher value of the Ni–N(Im) stretching mode (see Table 3). The spectral features and assignment of the other mode vibrations are listed in the ESI.†

The Raman spectra of the metal complexes show an intense band located between 2192 and 2184 cm^{-1}, assigned to the equatorial CN stretching mode. Generally, the IR spectra of metal nitroprussides with 3D structures show a single band in the CN stretching region, indicating that both equatorial and axial CN groups are linked to the metal center. The IR and Raman bands in the CN stretching region with corresponding assignments are presented in Table 3. The IR spectra of the materials under study show two bands assigned to the CN stretching mode, and these spectra confirm the presence of two types of CN groups, four equatorial CN ligands coordinated at both C and N ends, and one axial CN ligand that remains unbound at the N end, as was deduced by the crystal structure.

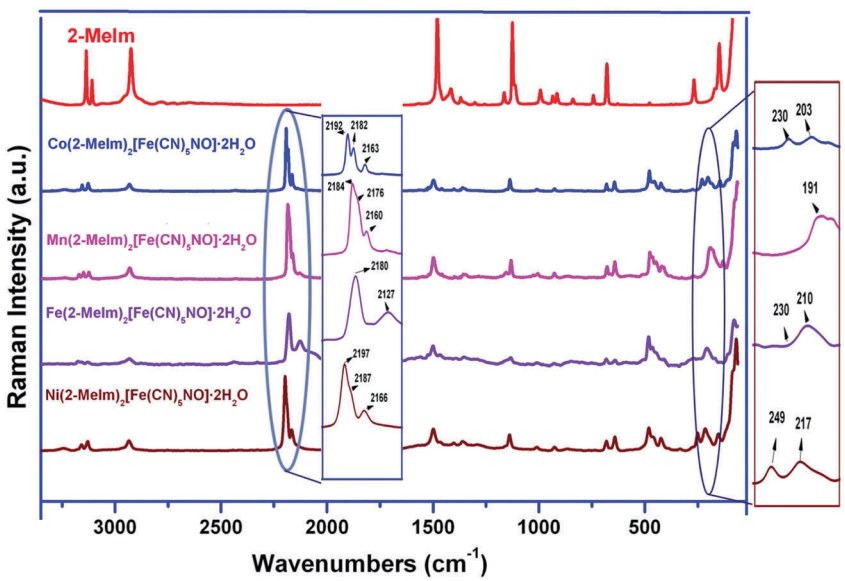

Fig. 4 Raman spectra of 2-methylimidazole and the solids T(2-MeIm)$_2$[Fe(CN)$_5$NO]·2H$_2$O (T = Co, Mn, Fe and Ni). Inset: Raman spectra of the CN stretching region between 250 and 150 cm^{-1}.

Table 3 Relevant IR and Raman frequencies for the solids $T(2\text{-MeIm})_2[Fe(CN)_5NO]\cdot 2H_2O$ (T = Co^{2+}, Fe^{2+}, Mn^{2+} and Ni^{2+})

$Mn(2\text{-MeIm})_2NP$		$Fe(2\text{-MeIm})_2NP$		$Co(2\text{-MeIm})_2NP$		$Ni(2\text{-MeIm})_2NP$		
IR	Raman	IR	Raman	IR	Raman	IR	Raman	Assignment[a]
—	2184	—	2186	—	2192	—	2197	ν(CN) eq
2173	—	2174	2179	2180	2179	2185	2188	ν(CN) eq
—	2160	2164	2161	2165	2163	2165	2165	ν(CN) ax
1934	—	1935	—	1936	—	1937	—	ν(NO)
—	191	—	239	—	230	—	249	νT–N(Im)

[a] ν: stretching modes; eq: equatorial ring; ax: axial ring; Im: imidazole ring.

The higher frequencies of the ν(CN) that appear at 2173, 2174, 2180 and 2185 cm^{-1} for complexes with T = Mn, Fe, Co and Ni, respectively, are assigned to the stretching vibration of the equatorial CN ligands that form the Fe–CN–T bridges. Since the CN stretching modes depend on the electronegativity, crystal field stability, oxidation state and coordination number of the metal center,[23] the ν(CN) of Fe(II)–CN–Ni(II) > Fe(II)–CN–Co(II) > Fe(II)–CN–Fe(II) > Fe(II)–CN–Mn(II). These results are in agreement with the results reported in Table 2 where the Mn(II) ion has a lower value of polarization power and a negative frequency shift for the ν(CN) stretching mode. The frequencies at around 2165 cm^{-1} in all of the complexes are assigned to the non-bridging CN stretching vibrations.

The bands located at around 1936 cm^{-1} in the IR spectra in the metal complexes are assigned to the NO stretching mode. The bands observed in the IR and Raman spectra below 1000 cm^{-1} are overlapped bands corresponding to ring modes and those within the nitroprusside ion. The bands observed at 667 cm^{-1} in the IR spectra of all of the metal complexes are attributed to the FeNO bending mode, and the weak bands at around 643 cm^{-1} are assigned to the Fe–N stretching mode. The IR bands observed at about 516, 446 and 427 cm^{-1} are assigned to δ(FeCN) and ν(Fe–C), respectively.

The UV-Vis diffuse reflectance spectra of all of the compounds as intimate mixtures in $BaSO_4$ are presented in the ESI.† The bands located in the visible region at 570 nm for Ni, 470 and 611 nm for Co, and 480 nm for Fe correspond to d–d transitions in an octahedral coordination. In the case of Mn, no d–d transitions are possible because it has half-filled 3d orbitals. In all of the complexes, the bands below 400 nm were assigned to metal–ligand electronic transitions within the nitroprusside anion.[24]

3.3. Thermal behavior

The thermal behavior of the solids $T(2\text{-MeIm})_2[Fe(CN)_5NO]\cdot 2H_2O$ (T = Co, Fe, Mn and Ni) was studied by Thermogravimetric (TG) and Differential thermal analysis (DTA) measurements in the temperature range 20–800 °C at 5° min^{-1} in an air flow. The thermal decomposition curves for the solids under study are shown in the ESI.† The TG curve for the complex with T = Mn shows that the compound crystallizes as a dihydrate, in agreement with the results derived from the crystal structure and IR data. The first step in the thermal decomposition of $Mn(2\text{-MeIm})_2NP$ finishes at 90 °C and is attributed to the loss of two water molecules (Exp. mass loss: 7.65%, calc. 8.0%). The complex is thermally stable up to 200 °C, and it decomposes in two consecutive steps, the first one finishes at 303 °C with a mass loss of 27% (theoretical value: 26%) that can be attributed to the removal of two 2-MeIm ligands and one NO group. This decomposition step is accompanied by an exothermic peak located at 288 °C in the DTA curve. The second step finishes at 606 °C and corresponds to the elimination and oxidation of the CN groups to form a mixture of $MnFe_2O_4$ (PDF #01-074-2403) and MnO (PDF #01-075-0626) in a molar ratio of 1 : 1 as final products. These products were identified from PXRD data. The experimental mass loss (37%) is in agreement with that calculated (39%) for the complete removal of the ligands. The DTA curve shows a stronger exothermic peak at 346 °C attributed to the removal of CN groups.

The complex $Fe(2\text{-MeIm})_2[Fe(CN)_5NO]\cdot 2H_2O$ decomposes in three steps. The first one finishes at 87 °C and corresponds to the removal of two water molecules. The low temperature of the release of water molecules upon heating is in agreement with the zeolitic nature of these water molecules. Also, according to the IR data and the crystal structure, the water molecules are stabilized by hydrogen bonding interactions. The experimental mass loss (7.0%) is in accordance with the calculated value of 8.0%. The DTA curve shows an endothermic peak located at 60 °C, attributable to the dehydration process. The second step in the decomposition process is attributed to the loss of two 2-MeIm ligands (calc. 34%, found 33%). This is in agreement with the exothermic peak at 276 °C observed in the DTA curve. In the third mass loss, the complex decomposes gradually in the temperature range of 282–490 °C, with a loss of the NO ligand and five CN groups (calc. 24%, found 25%) to produce Fe_2O_3 as the final product, which was confirmed from IR and PXRD data (PDF #016-0895).

The curves of the thermal decomposition of the Co(II) and Ni(II) complexes exhibit four pronounced mass loss steps. The first decomposition step finishes at 103 and 97 °C for the Co and Ni complexes, respectively, and corresponds to the loss of two water molecules. The experimental mass loss obtained for Co (9.0%) and Ni (8%) is in accordance with the calculated values (8% for Co and Ni). These results are in agreement with the endothermic peak at 91 °C observed in the DTA curves for both complexes. Next, the degradation steps occur within the range 230–330 °C, and they are attributed to the removal of two 2-MeIm ligands, in two consecutive steps. In the last stage, NO and cyanide groups in the complex are decomposed. These steps are associated with the exothermic peaks on the DTA

curves at 389 and 424 °C. These peaks are associated with the decomposition and burning of the NO and cyanide ligands to form mixtures of spinel-type oxides and simple metal oxides.

3.4. Magnetic properties

DC magnetic susceptibility and magnetization measurements were performed for all of the reported compounds. In the case of susceptibility data, it was collected at 80 Oe in the range of 1.8–300 K (Fig. 5), while magnetization *vs.* magnetic field data was achieved at 1.8 K under applied fields up to 70 kOe (see the ESI†).

The Ni complex shows a χT value per Ni(II) ion at 300 K of 1.60 cm^3 K mol^{-1}. This value is in agreement with the expected one for $S = 1$ and $g = 2.50$. It should be remarked, at this point, the closed shell nature of the nitroprusside moiety. When the temperature is decreased, χT steadily decreases up to 10 K where it suddenly falls to a value of 0.77 cm^3 K mol^{-1} at the lowest temperature, 1.8 K. This overall behavior can be rationalized in terms of dominant antiferromagnetic interactions with, most probably, a local ion zero field splitting (ZFS) onset in the lowest temperature range, expected for Ni(II) ions. The FC–ZFC experiment at 80 Oe does not show any divergence in the range 1.8–300 K, discarding any long-range ordering. The χ^{-1} *vs.* T plot does not follow a Curie–Weiss law with a clear deviation from linearity, even at almost 100 K, suggesting the existence of more than one exchange interaction pathway (see the ESI†). The magnetization field dependence at 1.8 K shows clear saturation at 1.9 Nβ. This value is well below the expected 2.28 (gS) saturation value, further proving the existence of a sizeable ZFS contribution. No opening of the hysteresis plot is observed, confirming again the lack of long-range magnetic ordering.

In the case of the Co complex, the observed χT value (per Co^{2+}) ion at 300 K is 2.31 cm^3 K mol^{-1}. This value is somewhat higher than the expected one for $S = 3/2$ and $g = 2.0$ (1.87 cm^3 K mol^{-1}), but still in a reasonable range ($g = 2.5$), evidencing that the usual first-order orbital contribution to the magnetic moment in this ion is largely quenched. When the temperature is lowered, χT smoothly decreases to 5 K where it shows a more pronounced decrease to a final value of 1.16 cm^3 K mol^{-1} at 1.8 K. This overall behavior, as in the case of the Ni(II) complex, can be rationalized in terms of dominant antiferromagnetic interactions with, most probably, a local ion ZFS onset at the lowest temperature range. The FC–ZFC experiment at 80 Oe does not show any divergence in the range 1.8–300 K, discarding any long-range ordering. The χ^{-1} *vs.* T plot follows a Curie–Weiss law almost down to 30 K, below this temperature a clear deviation from linearity is observed (see the ESI†). The Weiss constant arising from data fitting is −20.4 K which can be related to an antiferromagnetic exchange interaction of about −6.0 cm^{-1} (zJ with $z = 2$ due to *cis* and *trans* neighbours). The magnetization field dependence at 1.8 K shows clear saturation at 1.6 Nβ. This value is well below the expected 3.0 (gS) saturation value, evidencing the existence of a sizeable ZFS contribution. No opening of the hysteresis plot is observed in agreement with a lack of long-range magnetic ordering.

The Fe complex shows a χT value (per Fe^{2+} ion) at 300 K of 2.7 cm^3 K mol^{-1}. This value is close to the expected one for $S = 2$ (high spin d^6 ion) and $g = 2.0$ of 3.0 cm^3 K mol^{-1}. The extremely smooth χT decrease upon lowering the temperature suggests that exchange interactions are rather moderate. Below 20 K, the χT plot decreases more pronouncedly up to 5 K, when it abruptly starts increasing again. This sharp minimum becomes evidence for an incipient ferromagnetic long-range ordering. No clear FC–ZFC divergence can be distinguished, and there is no hysteresis opening in the magnetization field dependence data. The existence of uncompensated spin arising from the competing exchange interaction within the 2D sheets can give rise to ferromagnetic inter-sheet magnetic ordering. It is clear from inspection of the complex structures that two different exchange pathways can operate: *cis* and *trans* ones through the bridging nitroprusside moieties. Independent of the interaction nature (unless both exchange pathways are ferromagnetic), spin frustration cannot be avoided, hence an overall non-zero magnetic moment must be reached within the 2D sheet (Fig. 6). The χ^{-1} *vs.* T plot follows a Curie–Weiss law almost down to 5 K, where the long-range ordering begins (see the ESI†). The Weiss constant arising from data fitting is −6.0 K, which can be related to an antiferromagnetic exchange interaction of about −2.0 cm^{-1} (zJ with $z = 2$ due to the *cis* and *trans* neighbours). The magnetization *vs.* magnetic field dependence at 1.8 K does not show saturation, instead a steadily linear increase is observed, with a maximum value at 70 kOe of 2.4 Nβ. This value is well below the expected saturation value even for $S = 3/2$, possibly due to a strong ZFS contribution. The smooth linear increase of the magnetization at high fields can be due to the onset of incipient long-range ordering.

Regarding the Mn complex, the overall magnetic behavior follows that of the Fe complex, but with clearer long-range magnetic ordering signatures. A clear divergence of the FC–ZFC plots is observed at a blocking temperature of *ca.* 35 K as well as a drastic increase of the χT plot below *ca.* 48 K. As discussed in the case of the Fe complex, a ferromagnetic inter-sheet interaction between non-compensated magnetic moments within the sheets may be the explanation for this magnetic ordering.

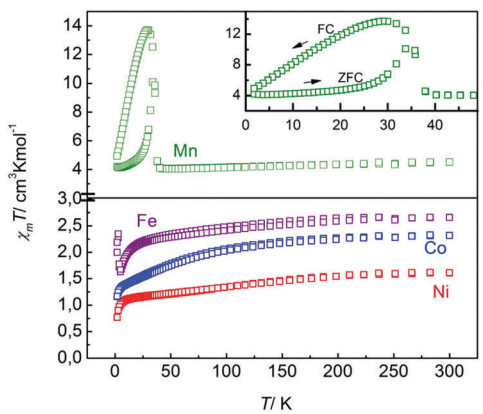

Fig. 5 χT *vs.* T FC–ZFC plots at 80 Oe in a 1.8–300 K temperature range.

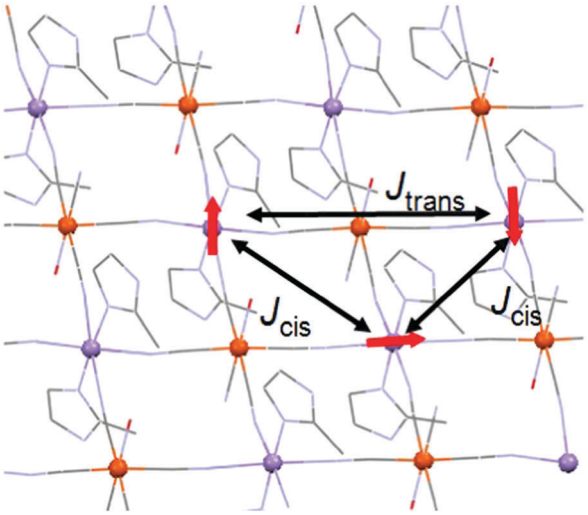

Fig. 6 Spin topology arrangement within the 2D sheets, emphasizing the spin frustration scenario.

The χT value at 300 K, 4.51 cm^3 K mol^{-1}, is in good agreement with that expected for S = 5/2 with g = 2.0 per Mn(II) ion, 4.37 cm^3 K mol^{-1}. The χT plot smoothly decreases down to 48 K where it abruptly increases to peak at a value of 13.8 cm^3 K mol^{-1} at 30 K due to the onset of long-range ordering. The χ^{-1} *vs.* T plot follows a Curie–Weiss law down to almost 35 K where the long-range ordering begins (see the ESI†). The Weiss constant arising from data fitting is −9.0 K, which can be related to an antiferromagnetic exchange interaction of about −3.0 cm^{-1} (zJ with z = 2 due to *cis* and *trans* neighbours). No hysteresis opening is observed at 1.8 K for the magnetization field dependence data.

Overall, all complexes with magnetic behavior can be understood in terms of dominant intra-sheet antiferromagnetic exchange interactions of moderate strength (between 1 and 10 cm^{-1}), as previously observed in other nitroprusside-bridged transition metal systems.[25–31] At very low temperatures, the onset of a local-ion ZFS contribution seems to be important. Only Fe and Mn compounds show long-range inter-sheet ferromagnetic ordering. In the case of Fe, the blocking temperature seems to be very low, but in the case of Mn this temperature is close to 35 K as inferred from the FC–ZFC experiment at low fields. The competing *cis*/*trans* exchange pathways afford a non-zero overall magnetic moment for the sheets allowing for the long-range ordering, probably mediated through non-covalent imidazole–imidazole interactions. Mn(II) offers the least local ion ZFS contribution as well as the highest magnetic moment per ion among the explored M(II) TMs. These properties can be related to the uniquely observed strongest long-range magnetic ordering.

4. Conclusions

In this study, four bimetallic coordination polymers containing the nitroprusside anion and 2-methylimidazole (2-MeIm) were synthesized and characterized using different spectroscopic techniques and thermal data measurements. Their crystal structures have been solved using PXRD data. The intercalated molecule is located in axial coordination positions for the metal T (Mn^{2+}, Fe^{2+}, Co^{2+}, and Ni^{2+}), thus resulting in a distorted octahedral coordination. The nitroprusside anion preserves its octahedral environment in which the Fe atom is six-coordinated to one nitrogen atom of the nitrosyl group and five carbon atoms of the cyanide ligands. Both coordination polyhedra are linked through a cyano bridge, and one cyanide ligand in the axial position remains unbridged. The existence of both CN ligands was confirmed from IR and PXRD data. In the interlayer region, 2-MeIm molecules interact between them through π-stacking interactions, which make the existence of the stable 3D structure of the solids formed possible. The magnetic behavior of all of the complexes can be understood in terms of dominant intra-sheet antiferromagnetic exchange interactions of moderate strength. At very low temperatures, the onset of the local-ion ZFS contribution seems to be important. Only Fe(II) and Mn(II) compounds show long-range inter-sheet ferromagnetic ordering. In the case of the Fe(II) complex the blocking temperature seems to be very low, but in the case of the Mn(II) complex this temperature is close to 35 K, as inferred from the FC–ZFC experiment at low field. The competing *cis*/*trans* exchange pathways afford a non-zero overall magnetic moment for the sheets allowing for the long-range ordering, probably mediated through non-covalent imidazole–imidazole interactions. Mn(II) offers the least local ion ZFS contribution as well as the highest magnetic moment per ion among the explored M(II) TMs. These properties can be related to the uniquely observed strongest long-range magnetic ordering.

Conflicts of interest

There are no conflicts to declare.

Acknowledgements

The authors thank SCAIT (D542/2), CONICET (PIP 11220130100651CO and PIP 0205), ANPCyT (PICT 2013-0697 and PICT 2016-0226) for financial support. A. D. S. thanks CONICET for the fellowship. R. E. C. thanks CONICET (PIP 11220120100360), ANPCYT (PICT 2012-3079) and SECYT-UNC (Res. 366/16) for financial support. This study was partially supported by the CONACyT (Mexico) projects 2013-05-231461 and CB-2014-01-235840. The help of A. R. Rodriguez for the magnetic data recording is greatly recognized.

References

1 A. Corma, H. García and F. X. Llabrés i Xamena, *Chem. Rev.*, 2010, **110**, 4606.
2 K. C. Stylianou, R. Heck, S. Y. Chong, J. Basca, J. T. A. Jones, Y. Z. Khimyak, D. Bradshaw and M. J. Rosseinsky, *J. Am. Chem. Soc.*, 2010, **132**, 4119.

3 K. Das, S. Mendiratta, A. Datta, M. J. Gajewska, E. Garribba, T. Akitsu and C. Sinha, *ChemistrySelect*, 2016, **1**, 2192.
4 Y. Li, K. Liu, W. J. Li, A. Guo, F. Y. Zhao, H. Liu and W. J. Ruan, *J. Phys. Chem. C*, 2015, **119**, 28544.
5 R. E. Morris and P. S. Wheatley, *Angew. Chem., Int. Ed.*, 2008, **47**, 4966.
6 S. Ferlay, T. Mallah, R. Ouahes, P. Veillet and M. Verdaguer, *Nature*, 1995, **378**, 701.
7 J. Werner, T. Runčevski, R. Dinnebier, S. G. Ebbinghaus, S. Suckert and C. Näther, *Eur. J. Inorg. Chem.*, 2015, 3236.
8 M. González, A. A. Lemus-Santana, J. Rodríguez-Hernández, M. Knobel and E. Reguera, *J. Solid State Chem.*, 2013, **197**, 317.
9 V. Niel, J. M. Martinez-Agudo, M. C. Muñoz, A. B. Gaspar and J. A. Real, *Inorg. Chem.*, 2001, **40**, 3838.
10 G. Agustí, S. Cobo, A. B. Gaspar, G. Molnár, N. O. Moussa, P. A. Szilágyi, V. Pálfi, C. View, M. C. Muñoz, J. A. Real and A. Bousseksou, *Chem. Mater.*, 2008, **20**, 6721.
11 P. D. Southon, L. Liu, E. A. Fellows, D. J. Price, G. J. Halder, K. W. Chapman, B. Moubaraki, K. S. Murray, J. F. Létard and C. J. Kepert, *J. Am. Chem. Soc.*, 2009, **131**, 10998.
12 M. González, A. A. Lemus-Santana, J. Rodríguez-Hernández, C. I. Aguirre-Velez, M. Knobel and E. Reguera, *J. Solid State Chem.*, 2013, **204**, 128.
13 F. Echeverría, A. A. Lemus-Santana, M. González, J. Rodríguez-Hernández and E. Reguera, *Polyhedron*, 2015, **95**, 75.
14 H. Osiry, A. Cano, A. A. Lemus-Santana, A. Rodríguez, R. E. Carbonio and E. Reguera, *J. Solid State Chem.*, 2015, **230**, 374.
15 D. M. Gil, H. Osiry, A. Rodrígez, A. A. Lemus-Santana, R. E. Carbonio and E. Reguera, *Eur. J. Inorg. Chem.*, 2016, 1690.
16 D. Louer and R. Vargas, *J. Appl. Crystallogr.*, 1982, **15**, 540.
17 A. Le Bail, H. Duroy and J. L. Fourquet, *Mater. Res. Bull.*, 1988, **23**, 447.
18 G. M. Sheldrick, *Program for Crystal Structure Determination*, University of Göttingen, Germany, 1997.
19 R. A. Young, *The Rietveld Method*, Oxford University Press, New York, 1995.
20 J. Rodriguez Carvajal, *Physica B*, 1993, **192**, 55.
21 D. B. Mullica, D. F. Trippin and E. L. Sappenfield, *Inorg. Chim. Acta*, 1990, **174**, 129.
22 D. B. Mullica, D. F. Trippin and E. L. Sappenfield, *J. Coord. Chem.*, 1992, **25**, 175.
23 K. Nakamoto, *Infrared and Raman Spectra of Inorganic and Coordination Compounds. Part B, Applications in Coordination, Organometallic, and Bioinorganic Chemistry*, John Wiley, 2009.
24 P. T. Manoharan and H. B. Gray, *J. Am. Chem. Soc.*, 1965, **87**, 3340.
25 Z. Smekal, T. Maris and M. Korabik, *J. Coord. Chem.*, 2014, **67**, 3167.
26 E. V. Peresypkina and K. E. Vostrikova, *Dalton Trans.*, 2012, **41**, 4100.
27 C. Yang, Q. L. Wang, Y. Ma, G. T. Tang, D. Z. Liao, S. P. Yan, G. M. Yang and P. Cheng, *Inorg. Chem.*, 2010, **49**, 2047.
28 Y. S. You, J. H. Yoon, J. H. Lim, H. C. Kim and C. S. Hong, *Inorg. Chim. Acta*, 2007, **360**, 2523.
29 D. V. Shevchenko, S. R. Petrusenko, V. N. Kokozay, A. Tomkiewicz, J. Klak, J. Mrozinski, M. V. Krasovska, O. V. Shishkin and W. Linert, *Inorg. Chim. Acta*, 2007, **360**, 2846.
30 X. Y. Chen, W. Shi, J. Xia, P. Cheng, B. Zhao, H. B. Song, H. G. Wang, S. P. Yan, D. Z. Liao and Z. H. Jiang, *Inorg. Chem.*, 2005, **44**, 4263.
31 H. L. Shyu and H. H. Wei, *J. Coord. Chem.*, 1999, **47**, 319.